Liquid Crystals
Publication details, including instructions for authors and subscription information:
http://www.informaworld.com/smpp/title~content=t713926090

Testing experimental analysis techniques for liquid crystals using computer simulation

Martin A. Bates[a]
[a] Department of Chemistry, University of York, York YO10 5DD, United Kingdom

To cite this Article Bates, Martin A.(2005) 'Testing experimental analysis techniques for liquid crystals using computer simulation', Liquid Crystals, 32: 11, 1365 — 1377
To link to this Article: DOI: 10.1080/02678290500354505
URL: http://dx.doi.org/10.1080/02678290500354505

Liquid Crystals, Vol. 32, No. 11–12, November–December 2005, 1365–1377

Invited Article

Testing experimental analysis techniques for liquid crystals using computer simulation

MARTIN A. BATES*

Department of Chemistry, University of York, York YO10 5DD, United Kingdom; e-mail: mb530@york.ac.uk

(*Received 4 August 2005; accepted 25 August 2005*)

Computer simulation has been used widely over the last two decades to investigate the phase behaviour and physical properties of liquid crystal systems. Here we review studies in which simulations have been used to calculate information on the physical properties of liquid crystals in a pseudo-experimental way. We concentrate on the calculation of 'experimental data' from computer simulations, from which we can extract information on the structure and dynamics of the nematic and smectic A phases. Where relevant, these are compared with both existing theoretical and experimental results. In particular, routes between the raw experimental data and physical parameters such as the orientational order parameter are highlighted and their effectiveness investigated.

1. Introduction

Computer simulation has become widely used in the field of complex liquids and is an important tool for examining the structure and dynamics of condensed matter systems. This field resides midway between experiment and theory. Although simulations rely on theoretical models, the techniques used are not analytic. Rather, in a simulation we typically observe a model system over a period of time or over statistically relevant configurations and so perform an averaging process similar to that when measuring any quantity in an experiment, albeit in a computer and for a model system. In this sense, simulation is a bridge between experiment and theory. Here we concentrate on how structural and dynamic information can be determined from simulations, and how this can then be compared with experimental and theoretical data. In particular, we concentrate on simulations during which 'experimental' data is obtained that can be analysed in exactly the same way as the corresponding data from real systems, as a way of testing the analysis routes.

This review is limited to a molecular model for liquid crystals which Geoffrey Luckhurst has been instrumental in promoting; namely, the Gay–Berne model. Rather than repeat work already discussed in a previous review on the phase behaviour observed for the family of Gay–Berne systems [1], we shall concentrate on three computer 'experiments'. We should note that there have been many simulations in which physical properties have been determined; for example, quanitities such as the elastic constants [2, 3] and viscosities [4] have been obtained from simulations. However, here we are particularly interested in how simulations can help our understanding of the analysis of real experimental data rather than, say, just calculating the temperature dependence of the elastic constants for a particular model and comparing this with real data for typical systems [2, 3].

As we shall see, in some cases the raw data calculated from the simulations, such as the scattering patterns, can be compared directly with that obtained from real experiments. These comparisons can validate the assumption that our model system is similar to real systems. However, simulation results can be used in a more interesting and useful way. Since we know the location and orientation of every molecule in every configuration, computer simulation can also give a direct route to the exact value for characteristic structural properties such as the nematic order parameter. In a real experiment, this has to be determined indirectly from an experiment in which something is measured (such as the splitting in an NMR experiment), and the value of the order parameter inferred, often using an assumption, rather than being determined directly from the orientations which, of course, we have no way of knowing for a real system. This means that if we can determine 'experimental' data, such as the scattering pattern, for the model liquid crystal and analyse this using the same method as for real systems, then we have two routes to the final answer: one direct

Liquid Crystals
ISSN 0267-8292 print/ISSN 1366-5855 online © 2005 Taylor & Francis
http://www.tandf.co.uk/journals
DOI: 10.1080/02678290500354505

route and one indirect route, via the analysis route that is used to extract parameters from real systems. These computer experiments allow us to test the validity of any approximations used in the analysis, and whether quantitative or only qualitative data can be extracted from the real experimental results.

We begin, in the following section, with a brief introduction to the Gay–Berne potential and the phase behaviour observed for the particular model used for all three experiments. In § 3, a method to calculate X-ray scattering patterns from computer simulations is outlined. This section also includes a discussion of the scattering patterns obtained for the Gay–Berne model. In § 4 and 5, the translational and rotational dynamics for the model system, respectively, are considered. These sections also include discussions of the relevant simulation results and their comparison with experimental work where possible. Our conclusions are presented in § 6.

2. The Gay–Berne model

The Gay–Berne potential was developed more than twenty years ago, as a model for describing the interactions between two elongated rigid molecules [5, 6]. The origin of the potential owed much to the pioneering work of Corner [7] into the development of pair potentials for molecules. He noted that the Lennard–Jones 12–6 potential provided a good description of the potential between a pair of atoms and so could also be used to describe the interactions between larger molecules if their deviations from spherical symmetry were coded into the potential. Although his ideas worked reasonably well for small molecules such as the nitrogen dimer, the potentials were not suitable for more elongated molecules, especially those of length-to-breadth ratios characteristic of liquid crystals. Berne and Pechukas [5] and later Gay and Berne [6] developed Corner's idea into a more suitable form for longer molecules. They showed that the interaction potential between a pair of rigid, elongated molecules could be reasonably well represented in a Lennard–Jones 12–6 form by

$$U_{\mathrm{GB}}(\hat{\boldsymbol{u}}_i,\ \hat{\boldsymbol{u}}_j,\ \boldsymbol{r}) = 4\varepsilon(\hat{\boldsymbol{u}}_i, \hat{\boldsymbol{u}}_j, \hat{\boldsymbol{r}})\left[\left(\frac{\sigma_{\mathrm{s}}}{r-\sigma(\hat{\boldsymbol{u}}_i, \hat{\boldsymbol{u}}_j, \hat{\boldsymbol{r}})+\sigma_{\mathrm{s}}}\right)^{12} - \left(\frac{\sigma_{\mathrm{s}}}{r-\sigma(\hat{\boldsymbol{u}}_i, \hat{\boldsymbol{u}}_j, \hat{\boldsymbol{r}})+\sigma_{\mathrm{s}}}\right)^{6}\right] \quad (1)$$

where $\hat{\boldsymbol{u}}_i$ and $\hat{\boldsymbol{u}}_j$ are unit vectors describing the orientations of the two molecules and $\hat{\boldsymbol{r}}$ is a unit vector along the intermolecular vector $\boldsymbol{r}$, with $r=|\boldsymbol{r}|$. Unlike the scalar σ in the well known Lennard–Jones potential for atoms, the distance parameter $\sigma(\hat{\boldsymbol{u}}_i, \hat{\boldsymbol{u}}_j, \hat{\boldsymbol{r}})$ for elongated molecules should be dependent on the orientations of the two molecules and the intermolecular vector. This is written as

$$\sigma(\hat{\boldsymbol{u}}_i, \hat{\boldsymbol{u}}_j, \hat{\boldsymbol{r}}) = \sigma_{\mathrm{s}}\left[1-\frac{\chi}{2}\left(\frac{(\hat{\boldsymbol{u}}_i\cdot\hat{\boldsymbol{r}}+\hat{\boldsymbol{u}}_j\cdot\hat{\boldsymbol{r}})^2}{1+\chi(\hat{\boldsymbol{u}}_i\cdot\hat{\boldsymbol{u}}_j)}+\frac{(\hat{\boldsymbol{u}}_i\cdot\hat{\boldsymbol{r}}-\hat{\boldsymbol{u}}_j\cdot\hat{\boldsymbol{r}})^2}{1-\chi(\hat{\boldsymbol{u}}_i\cdot\hat{\boldsymbol{u}}_j)}\right)\right]^{-\frac{1}{2}}. \quad (2)$$

Although this looks complicated, it is just a way of coding the shape of the molecule into the orientation dependent contact separation. A key component of the potential is the anisotropy in the shape of the molecule, χ, which is dependent on the length-to-breath ratio, $\kappa=\sigma_{\mathrm{e}}/\sigma_{\mathrm{s}}$, where σ_{e} and σ_{s} are the length and breadth of the molecule, respectively, and defined by

$$\chi = \frac{\kappa^2-1}{\kappa^2+1}. \quad (3)$$

Similarly, the energy parameter $\varepsilon(\hat{\boldsymbol{u}}_i, \hat{\boldsymbol{u}}_j, \hat{\boldsymbol{r}})$ should also be orientation dependent; for brevity the corresponding equations are not presented here, but are available in the original paper [6] and an earlier review [1]. An important parameter entering this term is the ratio of the potential energy for a pair of molecules in the side-by-side arrangement compared with that in the end-to-end arrangement $\kappa'=\varepsilon_{\mathrm{s}}/\varepsilon_{\mathrm{e}}$. Two further parameters, μ and ν, allow some extra freedom when the potential is fitted to particular models. Thus the Gay–Berne potential depends on four unique parameters: κ, κ', μ and ν. Since there are an infinite number of possible parameterizations and a number of variations have been studied, we have introduced a mnemonic GB(κ, κ', μ, ν) to denote the different models [8]. Note that all quantities for simulations using this model are quoted in reduced units. For example, pressure is defined as $P^*=P\sigma_{\mathrm{o}}^3/\varepsilon_{\mathrm{o}}$, distance $r^*=r/\sigma_{\mathrm{o}}$, energy $E^*=E/\varepsilon_{\mathrm{o}}$, density $\rho^*=\rho\sigma_{\mathrm{o}}^3$, temperature $T^*=k_BT/\varepsilon_{\mathrm{o}}$, time $t^*=t(\varepsilon_{\mathrm{o}}/m\sigma_{\mathrm{o}}^2)^{\frac{1}{2}}$, scattering vector $Q^*=Q\sigma_{\mathrm{o}}=2\pi/r^*$, diffusion coefficient $D^*=D(m/\sigma_{\mathrm{o}}^2\varepsilon_{\mathrm{o}})^{\frac{1}{2}}$ and moment of inertia $I^*=I(\sigma_{\mathrm{o}}^2/m)$, where ε_{o} and $\sigma_{\mathrm{o}}(\equiv\sigma_{\mathrm{s}})$ are the energy and distance scaling parameters, respectively, and m is the mass of a molecule [1, 8, 9].

Simulations have been used to construct the phase diagrams for many variants of this model in which the parameters are varied. In addition, other molecular interactions, such as electrostatic potentials [10, 11], have been added to the standard model and other variants of the model, for example, an extension to biaxial molecules [12], have been proposed. As these have been reviewed elsewhere [1], we shall not discuss them here. Rather we shall concentrate on a single

parametrization that has been well studied, the GB(4.4,20,1,1) model [8, 9], as our basic model for typical liquid crystal systems. Note that these parameters were chosen to reflect those expected for real mesogenic molecules [13], rather than in the *ad hoc* way in which Gay and Berne originally chose to parameterize the model [6]. This version of the potential has a reasonably rich polymorphism, exhibiting the isotropic, nematic and smectic A phases common to many rod-shaped liquid crystals. There is also a possibility of a smectic B phase for this model, although the distinction between this phase and a crystal B phase is rather subtle in a simulation of a small system. The phase diagram of GB(4.4,20,1,1) [8, 9] is shown in Figure 1. To construct this phase diagram, a number of constant pressure simulations were performed for each pressure [9], varying the temperature between each run. The equation of state, along with orientational and translational order parameters, can be determined from these simulations and so the phase diagram can be constructed. We observe that at relatively low pressures (see Figure 1), the GB(4.4,20,1,1) mesogen undergoes a transition from the isotropic phase directly to a smectic A. At a higher pressure, a nematic phase is observed between these two phases. This model therefore gives us the chance to investigate two different phase sequences, SmA–*I* and SmA–*N*–*I*, using the same model. This means that any differences observed for the systems will be due only to density and temperature and hence to the phase behaviour, rather than differences in the model potentials.

Before we consider the computer experiments, as we have already discussed, simulations are particularly useful in that the locations and orientations of the molecules are known. This means that molecular snapshots can be used to characterize the phases. We should point out, of course, that although these are informative, they give only a subjective view of the structure of the phase, and should not be relied on to distinguish two phases. For example, it is difficult to distinguish a nematic and a smectic A phase by eye very close to the transition between these phases. To characterize the phase unambiguously, the relevant distribution functions and/or order parameters should be determined [8]. However, since they are useful for observing the differences in structure away from the transitions, we show snapshots of the isotropic, nematic and smectic A phases in Figure 2. The characteristic orientational order in the nematic phase is clear when compared with the isotropic, as is the layering in the smectic A compared with the lack of positional order in the nematic.

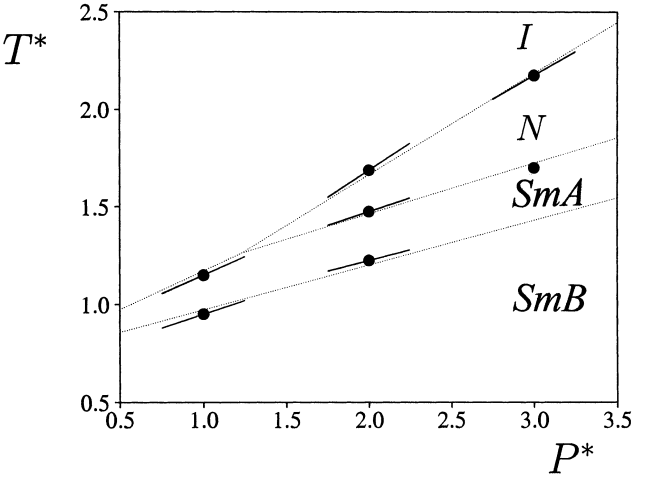

Figure 1. The phase diagram for the model mesogen GB(4.4,20,1,1). The points show the transition temperatures obtained from constant pressure Monte Carlo simulations and the solid lines show the phase boundaries calculated from the Clapeyron equation. (This figure is reproduced from [8, 9].)

3. X-ray scattering

X-ray scattering is an important technique for the study of liquid crystals [14] and is usually an invaluable tool

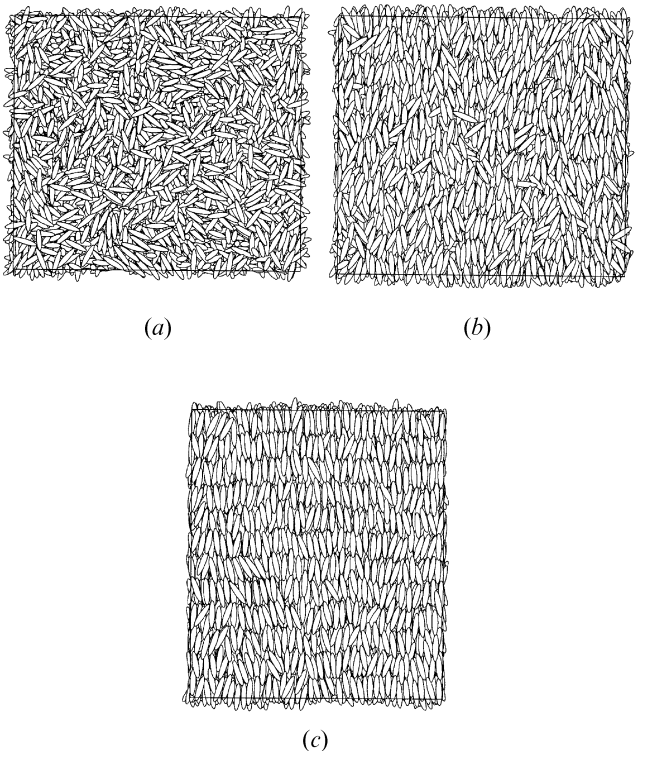

Figure 2. Snapshots of configurations taken from simulations of 16 000 molecules of (*a*) the isotropic, (*b*) the nematic and (*c*) the smectic A phase of the GB(4.4,20,1,1) model. (This figure is reproduced from [8, 9].)

for the unambiguous identification of the phase structure. Scattering patterns can also be used to determine structural parameters such as the average nearest neighbour separation and the smectic periodicity. Analysis of the arcs in scattering patterns should also lead to the singlet orientational distribution function [15]. The majority of experimental techniques can yield only the lower moments of this distribution, or order parameters, but not the distribution itself. However, as we shall see by making certain assumptions about the structure of the nematic phase, it is possible to determine the full singlet orientational distribution function from X-ray scattering patterns.

In principle, the calculation of the scattering pattern from a simulation of an atom-based model is straightforward. Since the positions $\boldsymbol{r}_j$ of the individual atoms $j=1, \ldots, N_a$ in the system are known, the total scattering intensity as a function of the scattering vector $\boldsymbol{Q}$ can be obtained [15, 16]

$$I_T(\boldsymbol{Q}) = \sum_{j,k=1}^{N_a} a_j(\boldsymbol{Q}) a_k(\boldsymbol{Q}) \exp\left(i\boldsymbol{Q}\cdot\boldsymbol{r}_{jk}\right) \quad (4)$$

where the sum is over all distinct pairs of atoms j and k, and $\boldsymbol{r}_{jk}$ is their separation vector; $a_j(\mathbf{Q})$ is the atomic scattering function. However, since we are using a molecular potential, the calculation of the scattering pattern is more problematic since individual atoms are not represented in the model; rather, the molecule is represented by a single object. To calculate the scattering pattern, we replace the spherical scattering sites used in the atomic calculations with elongated ones to represent the rod-like molecules in the Gay–Berne simulations [9, 17]. The scattering factor for such an elongated particle depends on the orientation of the ellipsoid with respect to the scattering vector in addition to the magnitude of the scattering factor $|\boldsymbol{Q}|$. A simple, although not unique, way to mathematically describe the dependence of the scattering factor for the elongated object is to stretch the scattering factor of a sphere [16] in a direction along the molecular long axis, to result in a scattering ellipsoid. Note that this approach also has the advantage that it is easily extendable to disc-shaped objects by squashing the sphere in a single direction. The equations necessary to calculate the scattering patterns based on a scattering ellipsoid approach are similar to those for the atomic case, but as we are now dealing with non-spherical scattering objects, the scattering factors necessarily depend on the orientations of the molecules with respect to the scattering plane; the full equations for these are given in [9, 17]. In particular, the total scattering intensity for a molecular system can be written in a form similar to that for the atomic case, equation (4), as

$$I_T(\boldsymbol{Q}) = \sum_{j,k=1}^{N_m} \mathcal{F}_j\left(\hat{\boldsymbol{u}}_j, \boldsymbol{Q}\right) \mathcal{F}_k\left(\hat{\boldsymbol{u}}_k, \boldsymbol{Q}\right) \exp\left(i\boldsymbol{Q}\cdot\boldsymbol{r}_{jk}\right) \quad (5)$$

in which the sum over pairs of distinct atoms is replaced with a sum over distinct pairs of molecules $j, k=1, \ldots, N_m$ and the orientation dependence of the molecular scattering function $\mathcal{F}_j\left(\hat{\boldsymbol{u}}_j, \boldsymbol{Q}\right)$ for molecule j is clear. Note that although this form (equations (4) and (5)) of the scattering intensity is particularly simple, for computational reasons it is better replaced by the product of two sums over a single molecular index [9, 17, 18].

To determine the scattering patterns for each phase, molecular dynamics simulations at state points corresponding to the smectic A, nematic and isotropic phases along the isobar at $P^*=2.0$ were performed for the GB(4.4,20,1,1) model [8]; these are $T^*=1.4$, $\rho^*=0.1932$ (smectic A), $T^*=1.6$, $\rho^*=0.1756$ (nematic) and $T^*=1.8$, $\rho^*=0.1562$ (isotropic). Full details of the molecular dynamics simulations for this model are described elsewhere [8, 9, 19, 20]. To be able to observe the fine details in the scattering patterns, large systems were found to be necessary. Here systems of 72 000 molecules in a slab geometry, extended in the x and z directions were used [17].

The intermolecular scattering patterns were obtained by analysing 50 well spaced configurations from the three simulations and are shown in figure 3. The broad ring observed at $T^*=1.8$, figure 3 (*a*), indicates the lack of long range orientational order in the isotropic phase. For the nematic phase, figure 3 (*b*), the anisotropy in the scattering pattern is evident by the break in this ring. By assuming a model for the packing of the molecules in the nematic phase [15], we can estimate the average molecular spacing. In contrast to the comparative laboratory experiment, we can compare the results using this assumed model with the exact pair distribution available directly from the simulation. The maximum intensity in the equatorial arc for the nematic phase occurs at $Q_\perp^* = 1.90\pi$ leading to an average side-by-side spacing $d_\perp^* = 1.05$. The random packed ($d_m^* = 1.12 d_\perp^*$) and close packed ($d_m^* = 1.15 d_\perp^*$) cylinders models describing the local packing in a liquid crystal phase [15] give the average spacing d_m^* to be 1.18 and 1.20, respectively, both of which are in good agreement with the position of the first peak in the pair distribution function at $r^*=1.21$ for the nematic phase [8]. Thus for the nematic phase it is not possible to distinguish between the random and close packed models; this is hardly surprising given the small difference between them and lack of translational structure in the nematic, which is responsible for the broadness of the nearest neighbour peak for the nematic

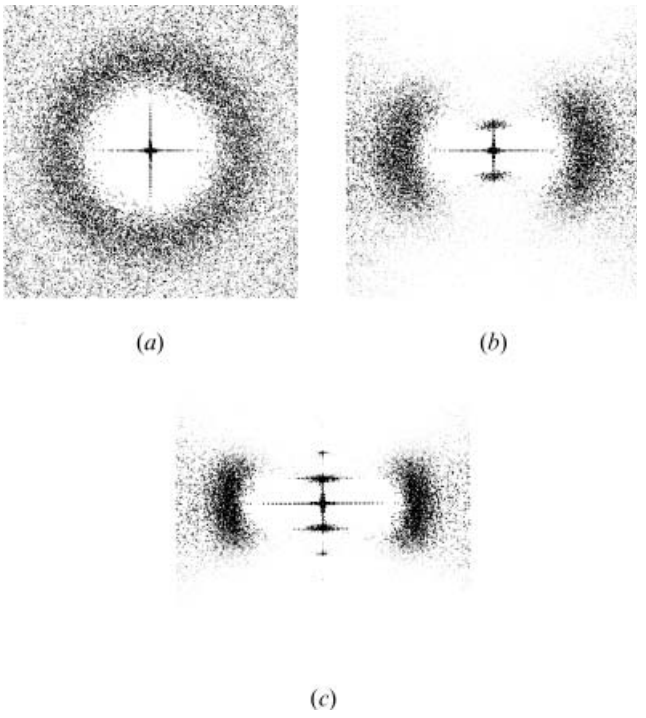

Figure 3. Q_{xz} intermolecular scattering patterns calculated for a system of 72 000 molecules along the isobar $P^*=2.0$ at temperatures (*a*) $T^*=1.8$ (isotropic), (*b*) $T^*=1.6$ (nematic) and (*c*) $T^*=1.4$ (smectic A). The patterns are calculated for scattering vectors Q_x^* and $Q_z^*=-3\pi \ldots +3\pi$. (This figure is reproduced from [9, 17].)

phase. In the scattering pattern for the nematic, there is also a peak shaped like a short arc along the meridional axis at $Q_\parallel^*=0.515\pi$. This peak corresponds to a spacing $d_\parallel^*=3.88$ or $0.88l^{*2}$, where l^* is the molecular length, which is similar to the values found for real nematics ($d_\parallel \approx 0.90l$) [15]. The origins for this peak are discussed elsewhere [14, 15, 17]. On cooling into the smectic A phase, figure 3 (*c*), the features in the scattering pattern do not change dramatically. The equatorial arcs are somewhat narrower and more intense, as expected given the higher orientational order at lower temperatures. We also observe that the meridional peak at $Q_\parallel^*=0.52\pi$ is much more intense than the equivalent peak in the nematic phase, and a second peak along the axis at $Q_\parallel^*=1.04\pi$ is also present. The layer spacing, d^*, calculated from the positions of these peaks is 3.82, which is in good agreement with the value of 3.85 estimated previously from the longitudinal distribution function $g_\parallel(r_\parallel^*)$ [8, 9].

So far we have seen that the scattering patterns for the isotropic, nematic and smectic A phases are similar to their counterparts in real experiments. This, of course, gives us confidence that the organization of the molecules in these phases in the model system are similar to those for real systems. In principle, this means that the scattering patterns could be determined from all simulations as a way of characterizing the phases observed in the simulation. However, given the large systems necessary and the long times needed to compute the patterns (see [9, 17]), this is not an effective route to the characterization of the phase behaviour. Indeed, determination of the order parameters and correlation functons is a much faster and simpler route to this information.

The scattering patterns obtained from the simulations are useful, however, when it comes to testing the theoretical assumptions made in the analysis of real scattering patterns. We have already seen that we can determine physical parameters such as the layer spacing in the smectic A phase and the average molecular spacing from the location of the various features in the scattering pattern. However, the defining characteristic of a liquid crystal is the long range orientational order, which is quantified by the singlet orientational distribution function. The relationship between the intensity distribution, $I(\theta)$, around the equatorial arc and the corresponding singlet orientational distribution function, $f(\beta)$, has been a subject of interest since, in principle, it should be possible to extract the latter from the former. However, it has not been possible to test the assumptions behind the proposed theories that are used to extract $f(\beta)$ for real liquid crystal systems, since this distribution cannot be determined using other experimental techniques and therefore the approximations in the analysis have not been tested for real data. However, with the simulations, this does now become possible since the orientational distribution can be obtained both directly from the simulation and indirectly from the scattering pattern of the model system, and so the accuracy of the different routes can be examined.

Two models have been proposed for extracting the singlet orientational distribution function, both of which rely on the assumption of locally aligned clusters. For a perfectly aligned but translationally disordered system, the equatorial scattering is confined to the equatorial plane [15]. This implies that the equatorial arcs observed in the scattering pattern of the nematic phase can be considered to arise from different domains in which perfect orientational order exists. The most simple approximation (Vainshtein's method) [21] is to identify the intensity around the arc, $I(\theta)$, as the singlet orientational distribution function, $f(\beta)$. This approach can be justified theoretically if the orientations of the molecules are confined to the plane defined by the director and the scattering vector, an approximation which becomes closer to reality at high orientational order. For nematic systems with high orientational order, the cone of angles within which the molecules

tend to align is narrow and so this should be a reasonable approximation. However, for real nematics, the cone of orientations is broad and so the approximation is expected to worsen as the system becomes less orientationally ordered. An improvement on this approximation was made by Leadbetter and co-workers [15, 22, 23] in which all orientations of the small aligned cluster are allowed. The angular intensity can then be related to the distribution function by [22, 23]

$$I(\theta)=\int_{\theta}^{\frac{\pi}{2}} f(\beta)\sec^2\theta\left(\tan^2\beta-\tan^2\theta\right)^{-\frac{1}{2}}\sin\beta\,\mathrm{d}\beta. \quad (6)$$

We note that, although both these methods are based on an aligned clusters assumption, this latter is often called the aligned clusters method. Schemes for inversion necessary for the aligned clusters model are given in [9, 17] and references therein.

Molecular dynamics simulations were performed at various temperatures to investigate the scattering patterns for nematic phases with varying degrees of orientational order, and the temperature dependencies of the scattering pattern and the angular intensity distributions are shown in figure 4. As the system is heated, the equatorial arcs become both broader and less intense until the scattering pattern consists of a single ring, characteristic of the isotropic phase (not shown). The angular intensity distribution was calculated from these patterns by integrating across the arc at fixed angle. Note that all distributions are normalized such that $\int f(\beta)\sin\beta\,\mathrm{d}\beta=1$ [9, 17]. For the isotropic phase (not shown), the angular intentsity distribution is found to be flat, as expected. In contrast, for the nematic the intensity distribution has a maximum at $\theta=0^\circ$ and decreases to a minimum at 90°, again as we expect since the molecules tend to align in a common direction. At the lowest temperature ($T^*=1.2$), the agreement between the aligned clusters method and the exact distribution determined in the simulation is very good. Vainshtein's approximation also gives a distribution of the correct shape but the maximum at 0° is relatively low, and so any order parameters calculated from this would be expected to be on the low side. Indeed, for comparative purposes we have calculated the nematic order parameter, $\overline{P_2}$, and the values are 0.63 ± 0.01 and 0.58 ± 0.01 for the aligned clusters and Vainshtein methods, respectively, whilst that measured in the simulation is 0.62 ± 0.01. As the temperature is increased, we observe a similar pattern. At the highest temperature in the nematic ($T^*=1.5$), the aligned clusters model gives a distribution which is again very close to the true distribution although again very slightly high, whereas Vainshtein's approximation gives a distribution which is too disordered. The corresponding values for $\overline{P_2}$ are 0.31 ± 0.01 (simulation), 0.31 ± 0.01 (aligned clusters) and 0.23 ± 0.01 (Vainshtein). Thus we can conclude that, of the two proposed routes to the singlet orientational distribution function, the aligned clusters model of Leadbetter and co-workers [22, 23] performs well over the entire nematic range, whereas the simple approximation of

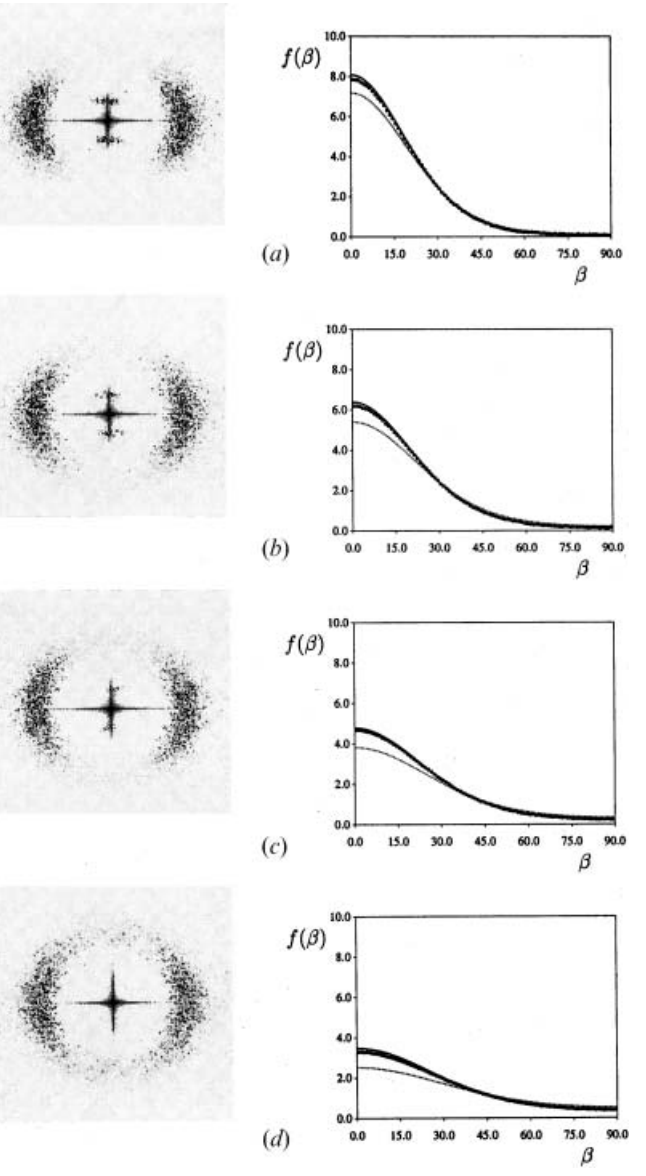

Figure 4. Q_{xz} intermolecular scattering patterns calculated for a system of 16 000 molecules along the isochore $\rho^*=0.16$ in the nematic phase at temperatures (*a*) $T^*=1.2$, (*b*) 1.3, (*c*) 1.4 and (*d*) 1.5. The patterns are calculated for scattering vectors Q_x^* and $Q_z^*=-3\pi\ldots+3\pi$. The corresponding (•) singlet orientational distribution function, (solid line) aligned clusters model result and (dotted line) Vainshtein's approximation for the distribution function are shown in each case. (This figure is adapted from [9, 17].)

Vainshtein [21] does not fare so well, especially when the orientational order is low. This is entirely as we expect, since the cone of angles within which the molecules tend to align becomes broadened with increasing temperature and so this approximation becomes gradually worse.

4. Translational diffusion

The characteristic of any liquid is the ability of the constituent molecules to flow. Liquid crystals are in no way different, albeit that their translational diffusion is affected by the orientational, and perhaps positional, order of the system. Diffusion in the nematic phase is reasonably well understood [24–26]. For the nematic phase, the diffusion coefficient parallel to the director, $D_{\|}$, is often found to be ~2–4 times larger than that perpendicular to the director, $D_{\perp}$. The relative difference in magnitude of the two principal diffusion coefficients can be readily linked theoretically with the extent of the orientational order in the nematic phase [25, 26]; note that these two theories give very different predictions depending on the extent of the order, especially in the high order limit. Computer experiments on both hard ellipsoidal bodies [26] and Gay–Berne systems [9] have been performed to determine the dependence of the ratio $D_{\|}/D_{\perp}$ on the nematic order parameter. For both types of model, the theory of Hess [26] appears to describe the dependence of $D_{\|}/D_{\perp}$ on $\overline{P_2}$ reasonably accurately. Typical results for the Gay–Berne model are shown in figure 5 [9]. Although the results seem to cluster around the theoretical result of Hess, we note that the ratio at higher order parameter for each series tends to dip below the theoretical prediction. This may well be due to instantaneous, local smectic-like structures appearing in the nematic before the transition to the smectic phase, which are not accounted for in the theory [9].

Diffusional behaviour for the smectic A phase is less obvious. The only difference between the smectic A and the nematic phases is the layering exhibited by the former. This should hinder diffusional motion parallel to the director while hardly affecting motion perpendicular to it. Thus the layering should lead to a decrease in $D_{\|}$ but not influence $D_{\perp}$, leading to a possible inversion of the ratio $D_{\|}/D_{\perp}$. Here we shall use simulation to test the validity of analytic theories of translational diffusion that allow for the influence of the layer structure of the smectic A phase on the motion parallel to the director, from which the barrier for diffusion between the layers can be extracted.

To investigate translational diffusion in the liquid crystalline phases of GB(4.4,20,1,1), we have used molecular dynamics simulations to study a number of

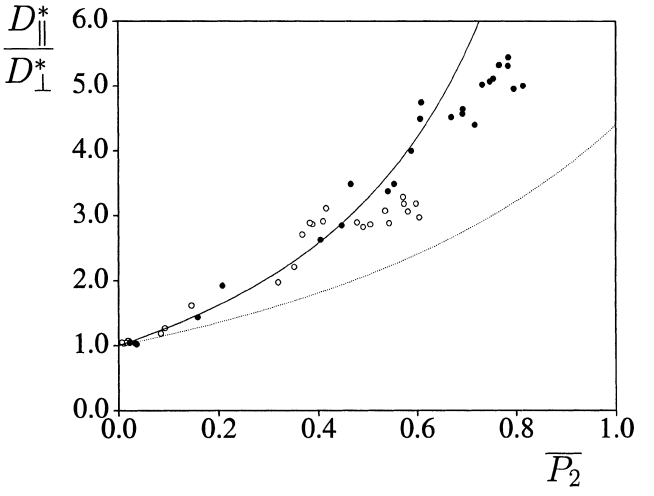

Figure 5. The anisotropy ratio of the diffusion coefficients ($D_{\|}^*/D_{\perp}^*$) plotted against the second rank orientational order parameter $\overline{P_2}$ from the simulations ($\hat{}$) at a constant density $\rho^*=0.16$ and (•) at a constant temperature $T^*=1.60$. Also shown are the predictions of Chu and Moroi [25] (dotted line) and Hess [26] (solid line). (This figure is reproduced from [9].)

state points taken from the two different isobars. We use a large system of 16 000 molecules as, for such large systems, the motion of the director is extremely slow and so the director is essentially stationary during the time taken for a molecule to diffuse over a distance comparable to the molecular length. Indeed, for such systems the director orientation remains constant over much longer timescales such that end-over-end rotation (see § 5) can also be studied in a fixed laboratory frame [27]. This is not the case for smaller systems of the order of a few hundred molecules, where the rotational motion of a single molecule necessarily has a larger effect on the orientation of the director. Full details of the simulations are given elsewhere [9, 19, 20, 27].

The diffusion coefficient for an isotropic liquid can be calculated from either a Green–Kubo formula, involving the integration of the velocity autocorrelation function, or from the time gradient of the mean squared displacement [28, 29]. These results are readily extended for anisotropic liquids. For example, the components of the anisotropic diffusion tensor can be determined from the slope of the mean square displacement versus time, resolved along directions parallel and perpendicular to the director, using an anisotropic version of the well known Einstein relation

$$2D_{\|} = \lim_{t\to\infty} \frac{\partial}{\partial t}\langle \Delta r_{\|}^2(t)\rangle$$
$$2D_{\perp} = \lim_{t\to\infty} \frac{\partial}{\partial t}\langle \Delta r_{\perp}^2(t)\rangle \qquad (7)$$

in which $\langle \Delta r_{\parallel}^2(t) \rangle$ and $\langle \Delta r_{\perp}^2(t) \rangle$ are the resolved components of the mean square displacement,

$$\begin{aligned} \langle \Delta r_{\parallel}^2(t) \rangle &= \langle \big(r_{\parallel}(t) - r_{\parallel}(0)\big)^2 \rangle = \langle |r_z(t) - r_z(0)|^2 \rangle \\ \langle \Delta r_{\perp}^2(t) \rangle &= \langle \big(r_{\perp}(t) - r_{\perp}(0)\big)^2 \rangle = \langle |r_x(t) - r_x(0)|^2 \rangle \\ &= \langle |r_y(t) - r_y(0)|^2 \rangle \end{aligned} \tag{8}$$

where we have assumed that the z-axis defines the director orientation. Note that $r_{\perp}(t) - r_{\perp}(0)$ is the distance travelled in time t along a particular direction perpendicular to the director, and not the total distance travelled in the perpendicular plane [9]. Since we are primarily interested in the uniaxial nematic and smectic A phases, we report a single perpendicular diffusion coefficient which was obtained by taking advantage of the phase symmetry by averaging over two mutually orthogonal directions in the perpendicular plane. Similar extensions are available for the Green–Kubo route to the diffusion constants [20].

In a solid, the temperature dependence of the diffusion coefficient can be described by the Arrhenius equation,

$$D = D' \exp(-E/RT) \tag{9}$$

where E is the activation energy or the height of the potential barrier over which a particle must jump to move from one lattice site to another. The structural disorder of liquids implies that there is no such precise meaning for E in liquid phases. Nonetheless, equation (9) is found to give a good description of experimental data measured for many isotropic liquids. As liquid crystals are observed between the solid and the liquid phases, it is reasonable to assume that an Arrhenius-type law will also hold for these phases and this indeed is found to be the case [24]. The temperature dependences of the diffusion coefficients $D_{\parallel}$ and $D_{\perp}$ can, therefore, be written as

$$\begin{aligned} D_{\parallel} &= D'_{\parallel} \exp\big(-E_{\parallel}/RT\big) \\ D_{\perp} &= D'_{\perp} \exp(-E_{\perp}/RT). \end{aligned} \tag{10}$$

Just as for isotropic liquids, the parameters in equations (10) do not have such a simple physical meaning as those in the solid. Indeed, for liquid crystals, the anisotropy in the diffusion tensor depends on the second rank orientational order parameter as we discussed earlier, which itself is strongly dependent on the temperature, especially near the $N-I$ transition; and so it is difficult to assign physical meaning to these parameters, since $E_{\parallel}$ and $E_{\perp}$ may also be temperature dependent. However, despite this apparent contradiction with the simple Arrhenius behaviour, these equations are found to fit the temperature dependence of the diffusion coefficients of real mesogens in many cases [24], presumably because the liquid crystalline phases are stable over only a small temperature range.

The temperature dependence of the diffusion tensor was determined along the two isobars; these are shown in figure 6. On cooling past the clearing point, we observe two rather different sets of results, depending on the phase behaviour of the system. At $P^*=1.0$, figure 6 (*a*), the isotropic phase undergoes a transition directly into the smectic A phase. The Arrhenius equation still gives an extremely good description of

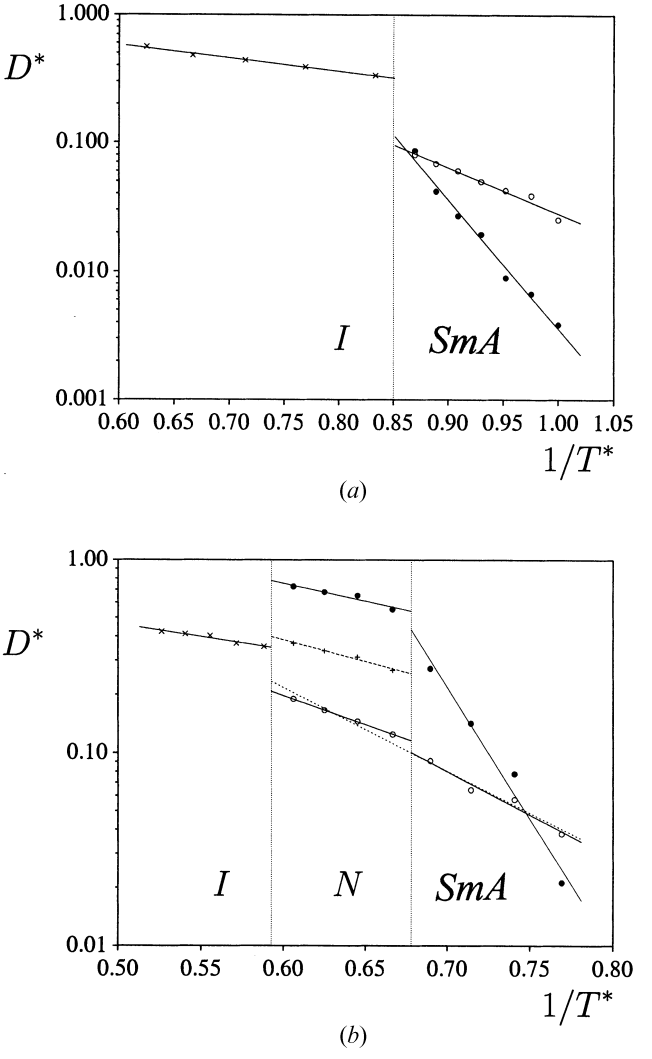

Figure 6. The temperature dependences of the diffusion coefficients along the isobars (*a*) $P^*=1.0$ and (*b*) 2.0. We show the (●) parallel and (○) perpendicular diffusion coefficients in the nematic and the smectic A phases and the average diffusion coefficients in the (×) isotropic and (+) nematic phases. The lines indicate the best fit for the Arrhenius law. (This figure is reproduced from [9, 20].)

the temperature dependencies of the parallel and perpendicular diffusion coefficients in this phase. Just below the SmA–*I* transition, we find that $D_{\parallel}^{*}$ and $D_{\perp}^{*}$ are approximately equal. However, the parallel diffusion coefficient decreases with decreasing temperature more rapidly than does the perpendicular coefficient. Thus we observe that, deep into the smectic A phase diffusion perpendicular to the director is faster than diffusion parallel to the director, and so we may conclude that the molecules diffuse within the layers more readily than between the layers. Thus the diffusional behaviour is, as it is sometimes called, smectic-like (somewhat misleadingly given that often $D_{\parallel}>D_{\perp}$ for smectic phases near a weak SmA$-N$ transition [24]), indicating that the diffusion is faster within the layer than between the layers; the opposite to this is nematic-like diffusion, where diffusion is more rapid along the director than perpendicular to it. We note that the diffusion coefficient drops by a factor of four or five at the SmA–*I* transition, indicating the far more viscous nature of the smectic A phase.

At $P^{*}=2.0$, a nematic phase is found between the smectic A and the isotropic phases. We again observe that the Arrhenius equation gives a good description of the temperature dependences of the diffusion coefficients in each phase, figure 6 (*b*). In the nematic phase, $D_{\parallel}^{*}$ is found to be larger than $D_{\perp}^{*}$ over the whole temperature range of the nematic, from which we may conclude that the molecules diffuse faster parallel to the director than perpendicular to it, and hence the diffusion is nematic-like, as we expect. This is entirely consistent with the theory of Hess [26] as we have already reported. As the $N-I$ transition is weak and the local molecular environment in these two phases is similar, we expect that there should be no difference between the extrapolated values of the isotropic diffusion coefficient and the average nematic diffusion coefficient at the transition. Indeed, these extrapolated values are very similar although we note that the average diffusion coefficient $\langle D^{*}\rangle=\frac{1}{3}(D_{\parallel}^{*}+2D_{\perp}^{*})$ just below the $N-I$ transition is slightly higher than the isotropic diffusion coefficient just above the transition; this is often seen for real systems [24]. On further cooling within the nematic phase, both $D_{\parallel}^{*}$ and $D_{\perp}^{*}$ are observed to decrease, as we expect given the temperature dependence of diffusion coefficients. We find that the negative slope for the perpendicular coefficient is very slightly larger than that for the parallel coefficient; this can be related to the increase in order as the system is cooled as we discussed earlier [20, 26]. At the transition into the smectic A phase, we observe a small jump in both the parallel and the perpendicular diffusion coefficients, although the slope of the Arrhenius plot does not change significantly for the perpendicular diffusion coefficient. Indeed, we find that a single Arrhenius fit gives a good description of $D_{\perp}^{*}$ over both the nematic and the smectic A temperature ranges, and so we conclude that diffusion perpendicular to the director is similar in both these phases. In contrast, we find a large change in the slope for the parallel diffusion coefficient. Just below the SmA–*N* transition, the diffusion is still nematic-like ($D_{\parallel}^{*}>D_{\perp}^{*}$) but, as the temperature is lowered, a cross-over point occurs at which this ratio inverts and $D_{\parallel}^{*}$ is then less than $D_{\perp}^{*}$ for all lower temperatures.

The two types of behaviour that we have found along the isobars $P^{*}=1.0$ and 2.0 are commonly observed in experiments on real mesogens. Indeed, both types of behaviour are often exhibited in the same homologous series. For example, Krüger [24] has studied translational diffusion in the liquid crystalline phases of a number of the 4-alkanoylbenzylidene-4′-aminoazobenzenes (C_n-BAA). The stability range of the nematic phase of C_6-BAA is quite wide and the Arrhenius plot is similar to that along the isobar $P^{*}=2.0$; they observe that $D_{\parallel}>D_{\perp}$, $D_{\parallel}\approx D_{\perp}$ or $D_{\parallel}<D_{\perp}$, depending on the temperature. In contrast, the nematic phase of C_{12}-BAA is very narrow and there is a large jump in the diffusion coefficients at the transition to the smectic A phase; throughout the smectic A range of C_{12}-BAA, $D_{\parallel}<D_{\perp}$.

Volino and co-workers [30, 31] have proposed a model to explain the temperature dependence of the parallel diffusion coefficient in both the nematic and the smectic A phases using a single Arrhenius fit, but taking into account an extra potential barrier due to the layering in the smectic A phase. It is assumed that the parallel diffusion coefficient in the nematic phase follows a simple Arrhenius behaviour, whilst the diffusion in the smectic A phase follows exactly the same Arrhenius-type process, that is, has the same temperature dependence as in the nematic. However, an extra term is included to account for the periodic potential experienced by a molecule diffusing parallel to the director in the smectic A phase. It is assumed that this potential can be written as a simple cosine function, in keeping with McMillan's theory of the smectic A phase [32] and the dominance of the first rank translational order parameter $\tau_1=\langle\cos(2\pi z/d)\rangle$ (c.f. [8]). The potential is written as

$$U(z)=-\frac{u}{2}\cos(2\pi z/d) \qquad (11)$$

where d is the layer spacing, z is the distance of the molecule from the centre of the layer and u is the barrier height. As there are no significant differences between the two phases at the microscopic level, the model

should hold in both the nematic and the smectic A phases of the same material with the same set of Arrhenius parameters, with the exception that the amplitude of the periodic potential is zero in the nematic phase. Under these assumptions, the diffusion coefficients can be obtained as [30, 31]

$$D_{\parallel} = D'_{\parallel} \frac{\exp(-E_{\parallel}/RT)}{I_0^2(xu/2RT)}$$
$$D_{\perp} = D'_{\perp} \exp(-E_{\perp}/RT) \qquad (12)$$

where I_0 is the zeroth order modified Bessel function of the first kind and x is equal to one in the smectic A phase and zero in the nematic phase.

In principle, this theoretical result should enable us to determine the potential for diffusing between one layer and the next. Since this can easily be determined in a simulation [9, 20], we can test the theory by determining the potential barrier both directly and indirectly, or by comparing the theoretical result for the temperature dependence of the diffusion coefficient with that measured in the simuation. To test the theory, we have taken two routes. The first is to determine the potential barrier for all temperatures in the smectic A phase, and average this to give a single value; note that a single temperature independent potential is assumed in the theory. The second is to replace the barrier height with the temperature dependent potential barrier [20]. The Arrhenius parameters $D'_{\parallel}*$ and $E^*_{\parallel}$ were obtained by fitting the data for the parallel diffusion coefficient in the nematic phase only. The resulting predictions for the smectic A phase are shown in figure 7. It is clear that the model in which the barrier height is independent of temperature cannot explain the temperature dependence of the parallel diffusion coefficient. Indeed, it does not matter which barrier height we choose, the assumption of a constant barrier height does not give a good representation of the data. In contrast, if the dependence of the barrier height on temperature is included, then the model gives a much more reasonable representation of the simulation data, although clearly this is far from perfect since the predicted diffusion coefficient is systematically larger than that actually measured in the simulation. We speculate that this is because as a molecule diffuses from one layer to the next, in addition to overcoming the sinusoidal layering potential, it must laterally push a small group of molecules apart to be able to squeeze between them. Clearly this will hinder the motion of the molecule parallel to the director, but is not taken into account in the theoretical model as it depends on the local in-plane structure of the smectic A phase; only the interlayer structure of the smectic A phase is taken into account in the theory. This should

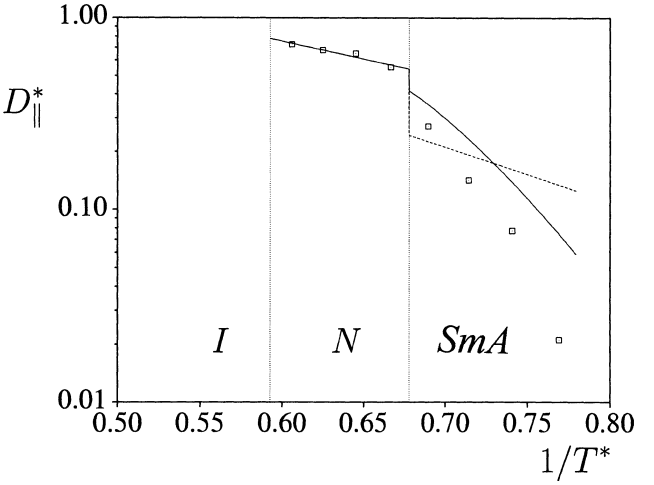

Figure 7. Fits of the cosine potential model for the parallel diffusion coefficient $D^*_{\parallel}$. The lines indicate the fits for the model with temperature dependent (solid line) and temperature independent amplitudes (dashed line). The Arrhenius parameters have been calculated for the nematic phase only and the barrier height(s) measured during the simulation. (This figure is reproduced from [9, 20].)

lead to a smaller diffusion coefficient than that predicted, as observed in the simulation.

We note that in order to test the theory for diffusion in the smectic A phase, we must have a prior knowledge of the layering potential. This cannot, of course, be obtained so readily from an experiment on a real mesogen. However, normally the opposite procedure is adopted; namely, the barrier height in the smectic A phase is determined from the diffusion data [30]. For our simulation results, this method would lead to an overprediction of the temperature dependent barrier height by approximately 25–30%. It is clear that this method cannot be used to determine the barrier height accurately. However, it does give a reasonable qualitative indication of how the barrier height changes with temperature. In turn, this should indicate whether the smectic order parameter, which is clearly linked to the height of the barrier, rapidly increases throughout the smectic A phase, or whether this is essentially constant throughout the smectic A temperature range.

5. Orientational dynamics

When investigating rotational dynamics, dielectric relaxation has proved to be a powerful technique [33–35]. In the uniaxial nematic phase, there are two principal components of the permittivity tensor, and the frequency dependence of the real and imaginary parts of both components can be used to explore the

orientational motion [36]. Of particular interest for nematics is the frequency dependence of the component parallel to the nematic director, $\tilde{\varepsilon}^*_{\parallel}(\omega)$, since, in principle, this contains information on the potential of mean torque responsible for the long range order of the constituent molecules [37].

According to the Maier–Saupe theory of nematics [37, 38], the potential of mean torque has the form

$$U(\theta) = -q\cos^2\theta \tag{13}$$

where θ is the angle between the molecular axis and the director and q is the height of the potential barrier. The presence of this barrier hinders rotational motion of the molecule about its short axes and thus leads to a longer relaxation time compared with that in the isotropic phase extrapolated to the same temperature. Meier and Saupe [39] introduced the idea of a retardation factor $g_{\parallel}=\tau_{\parallel}/\tau_o$ to describe the reduction in the relaxation rate; here $\tau_{\parallel}$ is the relaxation time for the parallel component of the permittivity tensor and τ_o is the equivalent (averaged) value in a hypothetical state with vanishingly small potential, that is, an isotropic state. Their extension of the Debye theory for nematics gives the retardation factor as a function of the barrier height as

$$g_{\parallel} = \frac{\exp(\sigma)-1}{\sigma} \tag{14}$$

where $\sigma=q/RT$. Martin *et al.* [40] used a more rigorous approach to obtain numerical results for the nematic relation time $\tau_{\parallel}$, and later an analytic theory which reproduced these numerical results well was deduced, in which the parallel retardation factor was found to be [41]

$$g_{\parallel} = \frac{\exp(\sigma)-1}{\sigma}\left[\frac{2\sigma}{1+\sigma}(\sigma/\pi)^{1/2}+2^{-\sigma}\right]^{-1}. \tag{15}$$

Both theories behave qualitatively as we expect: $g_{\parallel}>1$ for the nematic phase and $g_{\parallel}$ increases with increasing q. As the theories link experimental observables with the height of the potential barrier in the Maier–Saupe theory, in turn, this can be linked to the nematic order parameter. Therefore, measurement of the retardation factor allows us to calculate $\overline{P_2}$, under the assumption of the extended Debye theory. As in the previous two sections, we can test this assumption using simulation data; we can calculate σ or $\overline{P_2}$ both directly from the simulation and indirectly from the measured value of the retardation factor [27].

The rotational motion in the director-based laboratory frame was studied through the relevant function for relaxation parallel to the director, namely [35, 42]

$$c_{\parallel}(t^*) = \langle \cos\beta_o \cos\beta_{t^*}\rangle = \langle (\boldsymbol{u}_i(0)\cdot\boldsymbol{n})(\boldsymbol{u}_i(t^*)\cdot\boldsymbol{n})\rangle \tag{16}$$

where β_{t^*} is the angle made by the molecular long axis with the director at time t^* and $\boldsymbol{u}_i(t^*)$ and $\boldsymbol{n}$ are unit vectors describing the orientation of molecule i at time t^* and the director, respectively [27, 35, 42]. The correlation function $c_{\parallel}(t^*)$ is shown in figure 8 (*a*) in the isotropic and nematic phase of the GB(4.4,20,1,1) mesogen. The decay in this function is found to be well represented by a single exponential function [27, 36]

$$c_{\parallel}(t^*) = c_{\parallel}(0)\exp\left(-t^*\Big/\tau^*_{\parallel}\right) \tag{17}$$

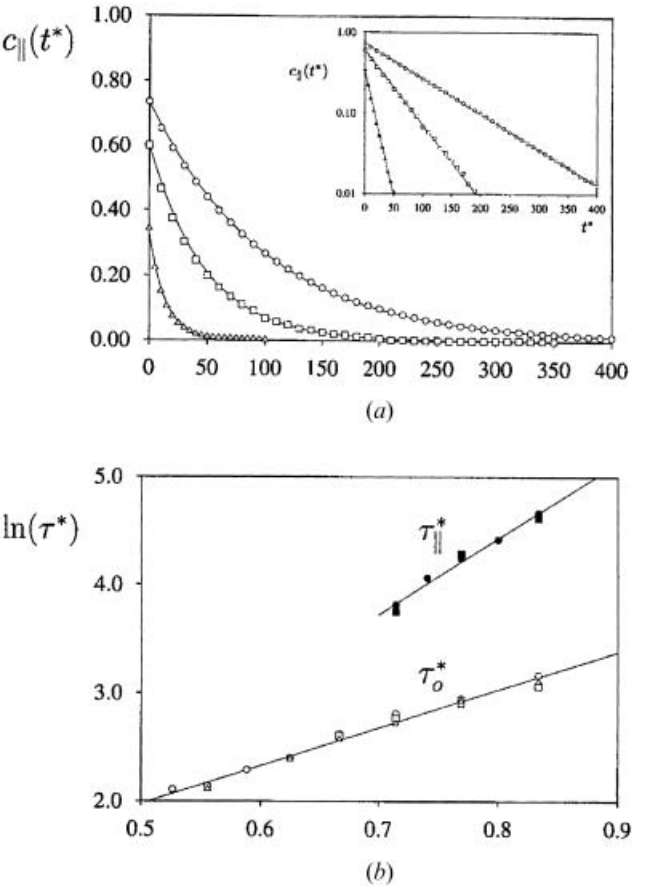

Figure 8. (a) The orientational correlation function $c_{\parallel}(t^*)$ for state points taken from the isochore $\rho^*=0.16$. From top to bottom: the nematic phase at $T^*=1.2$ and 1.4 and the isotropic phase at $T^*=1.6$. The inset shows the same data as a semi-logarithmic plot. (*b*) Arrhenius plot of the temperature dependence of the relaxation times $\tau^*_{\parallel}$ and τ^*_o. Open symbols denote data for the isotropic or supercooled isotropic phase; filled symbols denote data for the nematic phase. The straight lines indicate the best fit for the Arrhenius relationship. (This figure is reproduced from [27].)

in which the initial value is predicted [42] and found to be

$$c_{\parallel}(0) = \langle \cos^2 \beta \rangle = \frac{1}{2} + \frac{2}{3}\overline{P_2}. \tag{18}$$

This single exponential decay means that the frequency dependence of the imaginary component of $\tilde{\varepsilon}^*_{\parallel}(\omega)$ is a Lorentzian with a maximum occuring at $\tau^{*-1}_{\parallel}$, as found for nematic liquid crystals with an electric dipole parallel to the long axis. Once this decay was established, further simulations at different temperatures and densities were performed to determine the variation in the relaxation time $\tau^*_{\parallel}$. Of course, to calculate the retardation factor, $g_{\parallel}$, we need the relaxation time for a hypothetical state in which the potential of mean torque vanishes. For real systems, this is only obtainable by extrapolating results from the isotropic phase to temperatures in the nematic phase, assuming Arrhenius behaviour. In the simulations, an alternative is available. An isotropic phase can be supercooled and the relaxation times measured at the correct temperature but for an isotropic system; this only works because the relaxation times are relatively fast compared with the build-up of orientational order when the isotropic is quenched to a temperature corresponding to the nematic phase [27]. The relaxation times measured in this way, see figure 8 (*b*), indicate that the Arrhenius relationship for τ^*_{o} is perfectly valid. We also note that there is a distinct jump in the relaxation time at the transition to the nematic phase, as we expect for a first order transition, and that the relaxation times in the nematic are larger than those in the hypothetical state with vanishing potential of mean torque, again as we expect. Since we can calculate both $\tau^*_{\parallel}$ and τ^*_{o}, it is straightforward to calculate the retardation factor, $g_{\parallel}$, as a function of temperature and density. Thus the Maier–Saupe strength parameter can then be determined, assuming one of the models for reorientation in the nematic phase, equations (14) and (15). However, we can also calculate the Maier–Saupe strength parameter, σ, directly from the simulation [8, 9, 27]. This means that, for the simulation data, we can determine $g_{\parallel}$ as a function of σ making no implicit assumptions and this can then be used to investigate the accuracy of the theories.

The results for the isochore $\rho^*=0.16$ are shown in figure 9 (*a*). A similar plot in figure 9 (*b*) shows results for systems at higher densities and, hence, higher order parameters. It is clear from these results that the retardation factor for the GB(4.4,20,1,1) model increases with increasing potential of mean torque, as we expect. However, we notice that although this increase occurs, it is not in very good agreement with

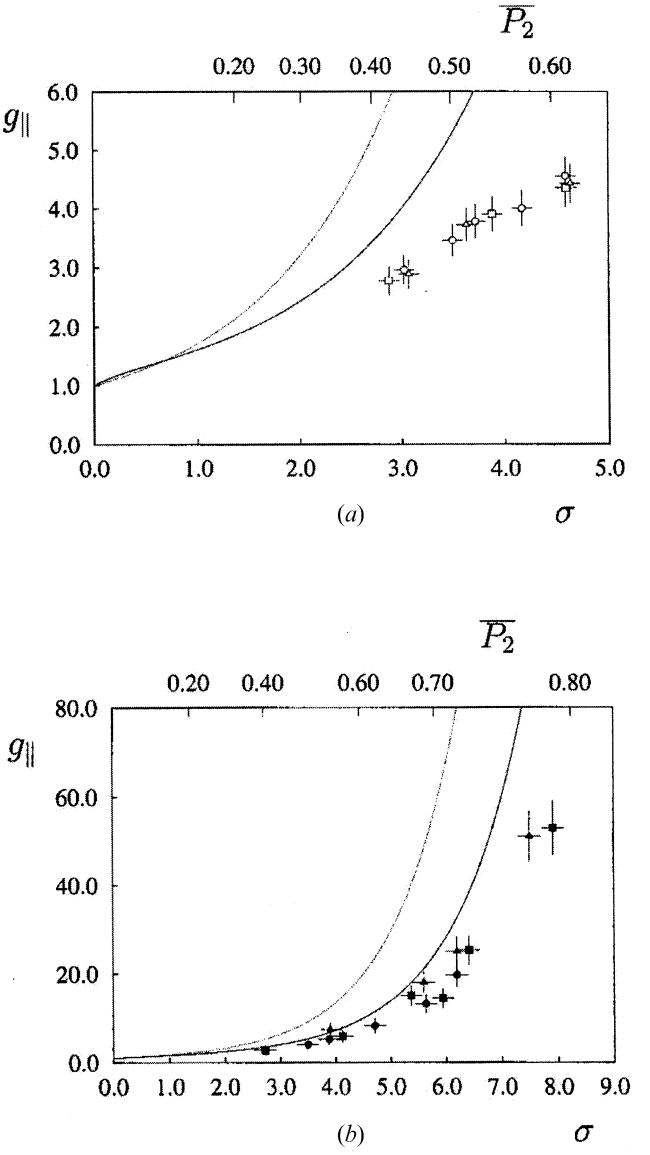

Figure 9. The retardation factor $g_{\parallel}$ as a function of the Maier–Saupe strength parameter $\sigma = q/RT$. (*a*) Along the isochore $\rho^* = 0.16$ for various system sizes; (*b*) for isochores $\rho^* = 0.17$, 0.18 and 0.19. The predictions of the Meier–Saupe theory are shown as the dotted line and Martin–Meier–Saupe theory by the solid line. Correpsonding values of $\overline{P_2}$ are shown along the top *x*-axis (non-linear scale). (This figure is reproduced from [27].)

either the theory of Meier and Saupe [39] or that of Martin *et al.* [40]. Indeed, both theories overpredict the retardation factor for any given value of σ. Aternatively, for a given measured retardation factor, the strength parameter, σ, and the order parameter, $\overline{P_2}$, are underestimated. Although the quantitative agreement is not good, the form of the increase does appear to be reasonable. The Martin–Meier–Saupe theory [40] typically underestimates σ by about 15%, which causes

an underestimation in $\overline{P_2}$ of about 0.1 for order parameters in the range 0.4 to 0.7, values typical of most real nematics. We also note that there is some density dependence of the retardaton factor; thus, different values of $g_{\|}$ are seen for the same value of σ at different densities. This may mean that free volume effects, which are ignored in the theory, may play a secondary role in the relaxation process.

6. Conclusions

We have shown that coarse-grained models, such as the Gay–Berne potential here, can reproduce the essential features of the phase diagrams of real liquid crystals. However, as well as being able to determine the phase diagram for these models, we can use them to understand, and investigate the accuracy of, the analysis of real systems. We have performed three types of computer experiment for the GB(4.4,20,1,1) model in which the structure, translational diffusion and orientational dynamics have been probed. In each case, the experimental results have been compared with those of real molecules where possible, and the simulations results have been analysed exactly as one would analyse real data. This, combined with certain theoretical assumptions, gives an indirect route to some property of the liquid crystal. Since this property can also be determined exactly from the simulation, the simulation route provides an opportunity to test the assumptions made in the theory and analysis.

References

[1] M.A. Bates, G.R. Luckhurst. *Struct. Bond.*, **94**, 65 (1999).
[2] J. Stelzer, L. Longa, H.-R. Trebin. *J. Chem. Phys.*, **103**, 3098 (1995).
[3] J. Stelzer, M.A. Bates, L. Longa, G.R. Luckhurst. *J. Chem. Phys.*, **107**, 7483 (1997).
[4] A.M. Smondyrev, G.B. Loriot, R.A. Pelcovits. *Phys. Rev. Lett.*, **75**, 2340 (1995).
[5] B.J. Berne, P. Pechukas. *J. Chem. Phys.*, **56**, 4213 (1972).
[6] J.G. Gay, B.J. Berne. *J. Chem. Phys.*, **74**, 3316 (1981).
[7] J. Corner. *Proc. R. Soc. London, Ser. A*, **192**, 275 (1948).
[8] M.A. Bates, G.R. Luckhurst. *J. Chem. Phys.*, **110**, 7087 (1999).
[9] M.A. Bates. PhD thesis, University of Southampton (1996).
[10] R. Berardi, S. Orlandi, C. Zannoni. *Chem. Phys. Lett.*, **261**, 357 (1996).
[11] M.A. Bates, G.R. Luckhurst. *Liq. Cryst.*, **24**, 229; M.A. Bates. *Liq. Cryst.*, **30**, 181 (2003) (1998).
[12] R. Berardi, C. Fava, C. Zannoni. *Chem. Phys. Lett.*, **297**, 8 (1998).
[13] G.R. Luckhurst, P.S.J. Simmonds. *Mol. Phys.*, **80**, 233 (1993).
[14] J.M. Seddon. In *Handbook of Liquid Crystals*, Vol. 1, D. Demus, J.W. Goodby, G.W. Gray, H.-W. Spiess, V. Vill (Eds). Chap. 8, Sect. 3, Wiley-VCH, Weinheim (1998).
[15] A.J. Leadbetter. In *The Molecular Physics of Liquid Crystals*, G.R. Luckhurst, G.W. Gray (Eds). Chap. 13, Academic Press, London (1979).
[16] A. Guinier, G. Fournet. *Small Angle Scattering of X-rays*. John Wiley, New York (1955).
[17] M.A. Bates, G.R. Luckhurst. *J. Chem. Phys.*, **118**, 6605 (2003).
[18] I.W. Hamley. PhD thesis, University of Southampton (1990).
[19] M.A. Bates, G.R. Luckhurst. *Chem. Phys. Lett.*, **281**, 193 (1997).
[20] M.A. Bates, G.R. Luckhurst. *J. Chem. Phys.*, **120**, 394 (2004).
[21] B.K. Vainshtein. *Diffraction of X-rays by Chain Molecules*. Elsevier, Amsterdam (1966).
[22] A.J. Leadbetter, E.K. Norris. *Mol. Phys.*, **38**, 669 (1979).
[23] A.J. Leadbetter, P.G. Wrighton. *J. Phys., Fr.*, **40**, C3:234 (1979).
[24] G.J. Krüger. *Phys. Rep.*, **82**, 229 (1982).
[25] K.-S. Chu, D.S. Moroi. *J. Phys., Fr.*, **36**, C1:99 (1975).
[26] D. Baalss, S. Hess. *Phys. Rev. Lett.*, **57**, 86 (1986).
[27] M.A. Bates, G.R. Luckhurst. *Mol. Phys.*, **99**, 1365 (2001).
[28] J.P. Hansen, I.R. McDonald. *Theory of Simple Liquids*. Academic Press, London (1976).
[29] M.P. Allen, D.J. Tildesley. *Computer Simulation of Liquids*. Clarendon Press, Oxford (1987).
[30] F. Volino, A.J. Dianoux. *Mol. Phys.*, **36**, 389 (1978).
[31] F. Volino, A.J. Dianoux, A. Heidemann. *J. Phys. Lett., Fr.*, **40**, 583 (1979).
[32] W.L. McMillan. *Phys. Rev. A*, **6**, 936 (1972).
[33] W.H. de Jeu. *Physical Properties of Liquid Crystalline Materials*. Gordon and Breach, New York (1980).
[34] H. Kresse. *Advances in Liquid Crystals*, G.H. Brown (Eds), Academic Press, London (1983).
[35] G. Williams. *The Molecular Dynamics of Liquid Crystals*, G.R. Luckhurst, C.A. Veracini (Eds). Chap. 17, Kluwer, Dordrecht (1994).
[36] P.L. Nordio, R. Rigatti, U. Segre. *Mol. Phys.*, **25**, 129 (1973).
[37] W. Maier, A. Saupe. *Z. Naturforsch*, **13a**, 564; W. Maier and A. Saupe. *Z. Naturforsch*, **14a**, 882 (1959); W. Maier and A. Saupe. *Z. Naturforsch*, **15a**, 287 (1960) (1958).
[38] G.R. Luckhurst. In *The Molecular Physics of Liquid Crystals*, G.R. Luckhurst, G.W. Gray (Eds). Chap. 18, Academic Press, London (1979).
[39] G. Meier, A. Saupe. *Mol. Cryst. Liq. Cryst.*, **1**, 515 (1966).
[40] A.J. Martin, G. Meier, A. Saupe. *Symp. Faraday Soc.*, **5**, 119 (1971).
[41] W.T. Coffey, D.S.F. Crothers, Yu.P. Kalmykov, J.T. Waldron. *Physica A*, **213**, 551 (1995).
[42] C. Zannoni, M. Guerra. *Mol. Phys.*, **44**, 849 (1981).